Investigating the effect of El Niño on nitrous oxide distribution in the Eastern Tropical South Pacific

Qixing Ji[1], Mark A. Altabet[2], Hermann W. Bange[1], Michelle I. Graco[3], Xiao Ma[1], Damian L. Arévalo-Martínez[1], and Damian S. Grundle[1,4]

[1]GEOMAR Helmholtz Centre of Ocean Research Kiel, Kiel, 24105, Germany
[2]School for Marine Science & Technology, University of Massachusetts Dartmouth, New Bedford, Massachusetts, USA
[3]Dirección General de Investigaciones Oceanográficas y cambio Climático, Instituto del Mar del Perú (IMARPE), P.O. Box 22, Callao, Perú
[4]Bermuda Institute of Ocean Sciences, St. George's, GE01, Bermuda

Correspondence to: Qixing Ji (qji@geomar.de)

Abstract. The open ocean is a major source of nitrous oxide (N_2O), an atmospheric trace gas attributable to global warming and ozone depletion. Intense sea-to-air fluxes of N_2O occur in major oceanic upwelling regions such as the Eastern Tropical South Pacific Ocean (ETSP). The ETSP is influenced by the El Niño-Southern Oscillation that leads to inter-annual variations of physical, chemical and biological properties. In October 2015, a strong El Niño event was developing in the ETSP; we conduct field observation to investigate (1) the N_2O production pathways and associated biogeochemical properties, and (2) the effects of El Niño on water column N_2O distributions and fluxes using data from previous non-El Niño years. Analysis of N_2O natural abundance isotopomers suggested that nitrification and partial denitrification (nitrate and nitrite reduction to N_2O) were occurring in the near surface waters; indicating that both pathways contributed to N_2O effluxes. Higher than normal sea surface temperatures were associated with a deepening of the oxycline and the oxygen minimum layer. Within the shelf region, surface N_2O supersaturation was nearly an order of magnitude lower than those of non-El Niño years. Therefore, a significant reduction of N_2O efflux (75 – 95 %) in the ETSP occurred during the 2015 El Niño. At both offshore and coastal stations, the N_2O concentration profiles during El Niño showed moderate N_2O concentration gradients, and the peak N_2O concentrations occurred at deeper depths during El Niño years; this was likely the result of suppressed upwelling retaining N_2O in subsurface waters. Water-column inventories of N_2O within the top 1000 m were up to 160% higher than those measured in non-El Niño years, indicating subsurface N_2O during El Niño could be a reservoir for intense N_2O effluxes when normal upwelling is resumed after El Niño.

1 Introduction

The El Niño-Southern Oscillation (ENSO) is a naturally occurring decadal climate cycle that affects the oceanic and atmospheric conditions across the equatorial Pacific (Philander, 1983). A pronounced effect of ENSO in the ocean is the

redistribution of heat flux across the tropical and subtropical Pacific. Generally, the ENSO cycle can be divided into three phases, El Niño, La Niña and neutral. During El Niño / La Niña years, higher / lower sea surface temperature and deepening / shoaling of the thermocline occur in the Eastern tropical South Pacific (ETSP) (Barber and Chavez, 1983). During El Niño years, upwelling is suppressed in the ETSP, and thus reducing upward nutrient fluxes to the surface waters and decreased primary production (Chavez et al., 2003; Ñiquen and Bouchon, 2004; Graco et al., 2017).

The ETSP is an oceanic region with intense sea-to-air flux of nitrous oxide (N_2O), a strong greenhouse gas and a potent ozone depleting agent in the 21st century (Ravishankara et al., 2009). Diverse microbial processes involved in the production and consumption of N_2O occur in the ETSP, a major oceanic oxygen minimum zone (OMZ) having wide range of O_2 concentrations spanning sub-nanomolar level at intermediate depths (Revsbech et al., 2009) to atmospheric saturation at the surface. In the presence of oxygen, N_2O is a by-product during the first step of nitrification, i.e. ammonium (NH_4^+) oxidation to nitrite (NO_2^-) (Anderson, 1964). Under suboxic and anoxic conditions, N_2O is produced via partial denitrification, i.e. NO_2^- reduction and nitrate (NO_3^-) reduction (Codispoti and Christensen, 1985). Partial denitrification can be mediated by denitrifying bacteria using NO_2^- and NO_3^- as substrates, as well as nitrifying bacteria using only NO_2^-, a process termed nitrifier-denitrification (Frame and Casciotti, 2010; Trimmer et al., 2016). The dominant biological sink of N_2O in the ocean is the last step of denitrification where N_2O is reduced to N_2 under anoxic conditions (Codispoti and Christensen, 1985). Recent investigations suggest that N_2O uptake by diazotrophs is another possible N_2O sink occurring at the surface waters (Farías et al., 2013; Cornejo et al., 2015). Its environmental significance awaits further exploration.

Research on the impact of ENSO on N_2O dynamics was initiated by the observation of significant reduction in oceanic N_2O effluxes during El Niño events (Cline et al., 1987; Butler et al., 1989). Recent model simulations demonstrated that ENSO events could induce lower denitrification rates, higher nitrification rates and lower N_2O fluxes (Mogollón and Calil, 2017; Yang et al., 2017), which could be related to changes in O_2 and organic matter availabilities that are critical environmental factors regulating N_2O production (Elkins et al., 1978; Farías et al., 2009; Arévalo-Martínez et al., 2015; Kock et al., 2016). Here we report water column hydrography, nitrogen biogeochemistry and N_2O distribution during October 2015 when a strong El Niño event (recurrence interval > 10 years) was developing (Stramma et al., 2016; Santoso et al., 2017). The natural abundance isotopomers of N_2O, i.e. the intramolecular configuration of stable isotopes (^{15}N vs. ^{14}N and ^{18}O vs. ^{16}O) were used to determine the pathways of N_2O production and consumption by a simple mass balance model outlined previously (Yamagishi et al., 2007; Grundle et al., 2017). Finally, we incorporated archived ETSP datasets to demonstrate contrasting hydrography and biogeochemistry as a result of a strong El Niño event so as to investigate the effects of on the surface and water column N_2O distributions.

2 Materials and Methods

2.1 Field sampling and laboratory measurements

The progress and the strength of El Niño was quantified by the Ocean Niño Index (ONI, Figure 1), defined as the running 3-month average sea surface temperature anomaly for the Niño 3.4 region in the east-central tropical Pacific (5˚S – 5˚N, 120˚W – 170˚W). The 2015-16 El Niño was a "strong El Niño event" indicated by ONI ≥ 0.5 °C from November 2014 to May 2016. This study was conducted on the ASTRA-OMZ SO243 cruise on board the R/V *Sonne* between the 5th and 22nd October 2015 from Guayaquil, Ecuador to Antofagasta, Chile (Figure 2a). In October 2015, the El Niño was still developing with ONI = 2.1 ℃, comparable to other strong El Niño events in 1972-73, 1982-83, 1997-98 (Stramma et al., 2016).

The sampling stations are categorized into offshore (Figure 2a in red polygon) and coastal (Figure 2a white polygon) according to their respective water depth: The coastal stations are shallower than 250 m whereas the offshore stations are > 3000 m in depth. Water samples were taken from a 24 × 10L-bottle CTD-rosette system. At every station, CTD-Niskin bottles collected water samples at 10 – 20 depths spanning the observed oxygen concentration range. The CTD system was equipped with two independent sets of sensors for temperature, conductivity (salinity) and oxygen measurements. Calibration for temperature, salinity and oxygen measurements were reported previously, with standard deviations of 0.002°C, 0.0011 PSU, and 0.8 µmol L^{-1} [O_2], respectively (Stramma et al., 2016). The detection limit of dissolved oxygen was ~ 3 µmol L^{-1}; the oxygen deficient zone (ODZ) was operationally defined as water parcels with [O_2] < 5 µmol L^{-1}, and the upper and lower oxycline boundary layer was defined as [O_2] = 20 µmol L^{-1} occurring above and below the ODZ, respectively. Saturation level of O_2 was calculated with in situ temperature and salinity according to Garcia and Gordon (1992). Dissolved NO_3^- and NO_2^- concentrations were measured at sea with an auto-analyzer (QuAAtro, Seal Analytical, Germany). Chemical analyses of NO_3^- and NO_2^- had detection limit of 0.1 and 0.02 µmol L^{-1}, respectively. For N_2O concentration measurements, triplicate samples were collected in 20 mL brown glass vials and were crimp-sealed with butyl stoppers and aluminum caps. Immediately following this, a 10 mL helium headspace was created and 50 µL of saturated mercuric chloride ($HgCl_2$) solution was added. After an equilibration period of at least 2 hours the headspace sample (10 mL) was measured by a gas chromatograph equipped with an electron capture detector (GC/ECD). The GC was calibrated on a daily basis using dilutions of two standard gas mixtures. The detailed GC/ECD setup and calculation of N_2O concentration were reported previously (Walter et al., 2006; Kock et al., 2016). For the N_2O concentration data of the 2015 cruise, the standard deviation of triplicate sampling was 1 – 8 %, generally < 2.5 nmol L^{-1}.

Water column N_2O saturation was quantified by the N_2O excess (ΔN_2O), defined as the concentration difference between measured and equilibrium values:

$$\Delta N_2O = [N_2O]_{measured} - [N_2O]_{equilibrium} \quad (1)$$

The N_2O equilibrium concentration was calculated according to Weiss and Price (1980) with in-situ temperature, salinity and the atmospheric N_2O dry mole fraction in the year of 2015, 328 ppb at 1 atmospheric pressure (Blasing, 2016). The N_2O efflux from the ocean to the atmosphere was calculated as the product of N_2O excess and gas transfer coefficient ($k_{w,}$ cm hr^{-1}) that was derived according to empirical relationship proposed by Wanninkhof (2014):

$$k_w = 0.251 \times U_{10}^2 \times \left(Sc/660\right)^{-0.5} \quad (2)$$

where U_{10} denotes wind speed (m s^{-1}) at 10 m above sea surface, Sc denotes the Schmidt number for N_2O under in-situ temperature (Wanninkhof, 2014).

Samples for natural abundance N_2O isotopomers were collected in 160 mL glass serum bottles with butyl stoppers and aluminum seals, and preserved with 100 µL of saturated $HgCl_2$. Isotopic measurements of N_2O were carried out at the University of Massachusetts Dartmouth following procedures previously reported (Grundle et al., 2017). In brief, dissolved N_2O was extracted by an automated purge-and-trap system and concentrated with liquid nitrogen. Interfering molecules such as H_2O and CO_2 were isolated from N_2O to increase measurement precision. A multi-collector isotope ratio mass spectrometer detected intact N_2O molecule's mass ratio of 45/44 and 46/44 and NO^+ fragment's mass ratio 31/30. Relative abundance of N_2O isotopomers were expressed using the delta notation (δX), defined as the relative difference between isotopic ratio (R) of sample and reference material:

$$\delta X = \frac{R_{sample}}{R_{reference}} - 1 \quad (3)$$

where X denotes $^{15}N_\alpha$, $^{15}N_\beta$ and ^{18}O, R denotes the $^{15}N/^{14}N$ at the central (α), terminal (β) nitrogen positions and $^{18}O/^{16}O$ at oxygen position of the N_2O molecule. The value of δX is expressed as permil (‰) deviation relative to a set of reference materials: atmospheric N_2 for $\delta^{15}N_{bulk}$ $\delta^{15}N_\alpha$ and $\delta^{15}N_\beta$ (Mohn et al., 2014), and Vienna standard mean ocean water (VSMOW) for $\delta^{18}O$. Therefore, mass ratios of 45/44, 46/44 and 31/30 determined $\delta^{15}N_{bulk}$ (conventionally $\delta^{15}N$), $\delta^{18}O$, and $\delta^{15}N_\alpha$, respectively. The $\delta^{15}N_\beta$, the relative abundance of N_2O molecule with ^{15}N substitution at terminal (β) position, was calculated by $\delta^{15}N_\beta = 2 \times \delta^{15}N_{bulk} - \delta^{15}N_\alpha$. Site preference (SP) are defined as follows:

$$SP = \delta^{15}N_\alpha - \delta^{15}N_\beta \quad (4)$$

Calibration of $\delta^{15}N_\alpha$-N_2O, $\delta^{15}N_\beta$-N_2O and $\delta^{18}O$-N_2O was accomplished using 4 certified standard gases (supplied by Joachim Mohn) encompassing the values reported here. The analytical precision of isotope measurements were ±0.07, 0.17, 0.36 and 0.18‰ for $\delta^{15}N_{bulk}$-N_2O, $\delta^{15}N_\alpha$-N_2O, $\delta^{15}N_\beta$-N_2O and $\delta_{18}O$-N_2O, respectively.

2.2 Additional datasets

The twice-weekly, 50-km resolution of sea surface temperature anomaly from NOAA's Satellite Coral Bleaching Monitoring Datasets (https://coralreefwatch.noaa.gov/satellite/ methodology/methodology.php) were used to quantify the sea-surface temperature difference of the ETSP during October 2015 relative to 1985 – 1993. For N_2O flux calculations,

instantaneous wind speed data at each of our sampling locations were acquired from shipboard metrological measurements. Seawater N_2O and oxygen concentrations from previous sampling campaigns in the ETSP were extracted from the MEMENTO database (Kock and Bange, 2015). Specifically, data from the following cruises were used for comparison between El Niño and non-El Niño years: NITROP-85 (February 1985), M77/3 (January 2009), Callao Time Series Transect (October 2011), M90 (November 2012), M91 (December 2012), AT26-26 (January 2015). The ONI of these years (1985, 2009, 2011, 2012, Figure 1) indicated that, 1985 and 2011 are considered as weak "La Niña" years, whereas 2009 and 2012 are considered "neutral" years. The MEMTNTO database did not archive N_2O data at the ETSP during previous El Niño events, and therefore we were not able to compare N_2O dynamics between two El Niño conditions. To facilitate the comparison, the 2015 and archived N_2O depth profiles were compared at three offshore and three coastal locations, each within a grid space of $0.75° \times 0.75°$ (see supplementary Table S1 for station coordinates). We assumed 5% of the mean N_2O concentrations as the analytical error for MEMENTO dataset.

3 Results

3.1 Hydrography, distribution of oxygen and inorganic nitrogen

A strong El Niño event during 2015-16 impacted the ETSP with a relatively high sea surface temperature anomaly, especially at the equatorial region (2 °S – 2 °N and 80 – 90 °W) where the highest anomaly between 3 and 5 °C was observed at offshore waters (Figure 2a). The El Niño-induced warming effect decreased southwards. Between 5 °S and 12 °S, the temperature anomaly was 2 – 3 °C. South of 12 °S the anomaly was generally < 1 °C. The shelf areas (7 °S – 14 °S) had a progressively lower temperature anomaly southwards; > 1.5 °C and < 1 °C north and south of 12 °S, respectively.

Five water masses, based on their thermohaline indices (Strub et al., 1998; Silva et al., 2009) were identified (Figure 2b). The northward-flowing Antarctic Intermediate water (AAIW, T = 3 – 5 °C, S ≈ 34.5) was found at depths below 1000 m. The Equatorial subsurface water (ESSW, T = 8 – 12 °C, S = 34.7 – 34.9) was near the Peruvian coast at depths between 300 and 400 m. Above the continental slope (water depth < 250 m), the colder Peru coastal water (PCW, T < 19°C, S ≈ 35) occupied 30 – 250 m, whereas the warmer subtropical surface water (STSW, T > 18.5 °C, S > 34.9) was found at depth < 30 m. The surface water north of the equator consisted of the tropical surface water (TSW), which had high temperature and low salinity (T > 25 °C, S < 33.5) due to excess precipitation. The October 2015 water column below 250 m had similar thermohaline properties compared to those of October – December 2012 (non-El Niño) that had been shown in an earlier study (Kock et al., 2016), except that October 2015 had warmer surface water.

Along the offshore section, the upper oxycline boundary ($[O_2]$ = 20 µmol L^{-1} isoline) was at 250 – 300 m along the equator at 85.5 °W, and the ODZ ($[O_2]$ < 5 µmol L^{-1}) appeared near 10 °S (Figure 3a). The southward shoaling of the oxycline, thickening of the ODZ and shoaling of the isoline with $[NO_3^-]$ = 20 µmol L^{-1} were observed south of 10 °S (Figure 3a and 3b), where the thickness of the ODZ was ~ 300 m. The top of the ODZ reached ~125 m between 13 °S and 16 °S. Significant accumulation of NO_2^- (>1 µmol L^{-1}) occurred south of 10 °S between 30 and 400 meters within the ODZ (Figure

3c), corresponding to lower NO_3^- concentrations (Figure 3b). The highest NO_2^- concentration (9.4 μmol L^{-1}) was recorded at 200 m at 15.7 ℃.

Along the coastal section, the surface (upper 10 m) O_2 concentrations were below saturation at all sampling stations (50 – 97 % saturation). Surface O_2 concentrations were 165 – 217 μmol L^{-1} north of 10 ℃ and gradually decreased to 135 – 190 μmol L^{-1} between 10°S and 12.5°S, and to 120 μmol L^{-1} south of 14 ℃ (Figure 3d). The shoaling of the 20 μmol L^{-1} O_2 isoline was observed south of 9 ℃. The top of the ODZ was found at 200 m, 150 m and 80 m at 11 ℃, 12 ℃ and 14 ℃, respectively. The surface NO_3^- concentrations were 11 – 23 μmol L^{-1} between 9°S and 16°S, and the 20 μmol L^{-1} NO_3^- isoline was at 0 – 20 m (Figure 3e). Water column NO_2^- concentrations at coastal stations were generally below 1 μmol L^{-1}, with the exception of the station at 14.0 ℃ where NO_2^- concentrations reached 1.2 μmol L^{-1} below 200 m (Figure 3f).

3.2 Water column N_2O concentrations and isotopes

Along the offshore section, the water column N_2O distributions showed a southward increase of surface N_2O concentrations and southward decrease of subsurface N_2O maxima (Figure 4a). The equatorial region (1 ℃ to 2.5 ℃, 85.5 ℃) had subsurface high N_2O concentrations (up to 93 nmol L^{-1}) at thermocline depths (200 – 550 m); water column $\delta^{15}N$, SP and $\delta^{18}O$ generally increased with depth (Figure 4b, 4c and 4d); at the subsurface N_2O concentration maximum, $\delta^{15}N$, SP and $\delta^{18}O$ were ~ 6 ‰, 13 – 17 ‰, and 45 – 50‰, respectively. Two N_2O concentration maxima were observed at stations south of 10 ℃ where the ODZ was formed. Near 10 ℃, two N_2O concentration maxima (70 ± 6 nmol L^{-1}) occurred between 200 and 600 m; and a local concentration minimum (~ 30 nmol L^{-1}) occurred within the ODZ at 400 m, associated with high $\delta^{15}N$ (8 – 10 ‰), SP (20 – 30‰) and $\delta^{18}O$ (60 – 70‰). Near 13°S, a shallow N_2O concentration maximum (~ 80 nmol L^{-1}) occurred at ~100 m, and a local N_2O concentration minimum (18 nmol L^{-1}) occurred at 350 m. Between 14 ℃ and 16 ℃, the lowest (< 10 nmol L^{-1}) N_2O concentrations were observed at 200 – 400 m within the ODZ, where the highest values of $\delta^{15}N$ (> 10 ‰), SP (30 – 40‰) and $\delta^{18}O$ (> 60 ‰) were observed.

Along the coastal section, a southward increase of surface N_2O concentration (20 nmol L^{-1} north of 11 ℃ and > 40 nmol L^{-1} south of 13 ℃) was observed, coinciding with southward shoaling of the ODZ (Figure 4e). Subsurface maximum N_2O concentrations were observed below 200 m near 10.7 ℃, and at 80 – 90 m south of 12 ℃, where ODZ was formed. The $\delta^{15}N$ in coastal waters were between 2.5 and 5 ‰, with lower values at stations south of 14 °S (Figure 4f). SP was lower (< 0 ‰) at the surface (< 10 m) near 9 ℃ and at 50 – 150 m near 11 ℃; higher SP (10 – 20 ‰) was observed south of 14 ℃ (Figure 4g). The $\delta^{18}O$ values were 45 – 60 ‰; higher $\delta^{18}O$ (> 55 ‰) were observed within the ODZ below 200 m at 14 ℃ and below 100 m at 15.3 ℃ (Figure 4h).

3.3 Excess N_2O and N_2O flux to the atmosphere

Both the offshore and coastal stations showed N_2O supersaturation in the top 10 m of surface water, and coastal stations had higher ΔN_2O concentrations (15 – 50 nmol L^{-1}) than those of offshore stations (4 – 8 nmol L^{-1}). Subsurface

ΔN_2O along the offshore section had higher concentrations (70 – 80 nmol L^{-1}) at the equatorial regions than ΔN_2O concentrations (40 – 60 nmol L^{-1}) at stations located south of 10 °S (Figure 5a). Near 15 °S, subsurface N_2O undersaturation was observed; ΔN_2O concentrations were -4 – 0 nmol L^{-1} at thermocline depths (200 – 400 m) within the ODZ ($[O_2] < 5$ µmol L^{-1}). Along the coastal section, a southward increase of surface and subsurface (50 – 200 m) ΔN_2O was observed (Figure 5b). Subsurface maximum ΔN_2O concentrations were > 60 nmol L^{-1}, and occurring at the periphery of ODZ (~ 200 m near 10 °S and < 100 m south of 12 °S). Undersaturation of N_2O ($\Delta N_2O < 0$) did not occur in any coastal stations. The N_2O fluxes from the coastal stations were 23 – 108 µmol m^{-2} d^{-1}, nearly two folds of the offshore fluxes (7 – 50 µmol m^{-2} d^{-1}, Figure 5c). The highest flux occurred at a coastal station at 14.4°S, 77.3°W, coinciding with the highest surface ΔN_2O (50 nmol L^{-1}).

4 Discussion

The ETSP is one of the world's major OMZs having active N_2O production and intense efflux to the atmosphere (Arévalo-Martínez et al., 2015; Kock et al., 2016). The gradient spanning from fully oxygenated conditions to anoxia creates suitable conditions for N_2O production and consumption, which causes the co-existence of water column N_2O supersaturation and undersaturation (Codispoti and Christensen, 1985). To identify the N_2O cycling pathways, we input N_2O isotopomer measurements into a simple mass balance model (section 4.1). Quantitative relationships linking O_2, NO_3^- and N_2O were examined to characterize the effect of oxygenation on N_2O production from NH_4^+ oxidation (section 4.2). Previously measured N_2O concentrations from the ETSP were extracted from the MEMENTO database (Kock and Bange, 2015) and were compared to data from this study to investigate the contrasting water column N_2O distribution and effluxes between El Niño and non-El Niño years (section 4.3), which would better constrain the natural variability of N_2O cycling in the ETSP.

4.1 N_2O cycling pathways inferred from natural abundance isotopic and isotopomeric signatures

The analyses of natural abundance isotopomers quantify the substitutions of nitrogen and oxygen isotopes occurring on the linear asymmetric N_2O molecule (Yoshida and Toyoda, 2000), and can be used to identify potential production and consumption pathways (Yamagishi et al., 2007; Grundle et al., 2017). The production of N_2O in an isolated water body follows mass conservation of the respective isotopes. The mass balance model proposed by Fujii et al. (2013) quantified the isotopic signature of N_2O produced within the water mass ($\delta_{produced}$) by the linear regression of the inverse N_2O concentration ($1/[N_2O]_{measured}$) and the observed isotope values ($\delta_{observed}$):

$$\delta_{observed} = \frac{1}{[N_2O]_{measured}} \times \left(\delta_{initial} - \delta_{produced}\right) \times [N_2O]_{initial} + \delta_{produced} \quad (6)$$

where $[N_2O]_{initial}$ and $\delta_{initial}$ refer to source water N_2O concentration and isotopic signature, respectively. It has been shown that SP is indicative of N_2O production pathways, because SP is independent of isotopic values of the substrates for N_2O production. Both culture and field studies demonstrated that N_2O production pathways of NH_4^+ oxidation and partial denitrification (including both nitrifier- and denitrifier-mediated denitrification) are associated with SP values of 30 ± 5 ‰ and 0 ± 5 ‰, respectively (Toyoda et al., 2011). Thus by determining $SP_{produced}$, N_2O production processes can be qualitatively characterized. We further identified four water bodies (coastal and offshore stations combined) from shallow to deeper depths with distinctive features such as O_2, NO_2^- concentrations and depths (Table 1) to discuss N_2O cycling pathways as follows.

(1) Upper oxycline and surface (Figure S1a): $[O_2] > 20$ μmol L^{-1}, $[NO_2^-] < 1$ μmol L^{-1}, and depth < 200 m. N_2O production from this water body could actively contribute to atmospheric efflux. The samples had variable SP values (-9 – 34 ‰); some coastal samples had low SP values (-5 to -9 ‰, Figure 4g), an isotopic signature of strong denitrifying activities demonstrated previously in culture (Winther et al., 2018) and river water (Mothet et al., 2013). The low $SP_{produced}$ (6.4±1.9) indicates that both nitrification and denitrification were sources of N_2O to the upper oxycline, with the majority appearing to come from denitrification. Given that the O_2 concentrations were too high for denitrification to proceed locally in the upper oxycline and the surface (Codispoti and Christensen, 1985), the SP signature of N_2O in this water body was a mixture of local nitrification and denitrification signal from the peak N_2O concentration depths (see below) as a result of active upwelling and upward diffusion in the ETSP (Haskell et al., 2015). Thus, denitrification and nitrification both contribute to N_2O effluxes in the ETSP-OMZ, consistent with a previous study which focused on the coastal regions between ~12 – 14 ℃ (Bourbonnais et al., 2017).

(2) N_2O peak (Figure S1b): $[O_2] = 5 – 20$ μmol L^{-1} and $[NO_2^-] < 1$ μmol L^{-1}, and depth = 45 – 500 m. The samples were from N_2O concentration maxima near the upper boundary of the ODZ. The $SP_{produced}$ is relatively low (8.3±3.0 ‰) at this suboxic water body ($[O_2] < 20$ μmol L^{-1}), which allowed N_2O production from denitrification while inhibited N_2O consumption (Bonin et al., 1989; Farías et al., 2009). The $SP_{produced}$ leads us to conclude that water column N_2O maximum was mainly attributed to partial denitrification (i.e. NO_2^- and NO_3^- reduction). This is consistent with previous ^{15}N tracer incubation experiments demonstrating that N_2O concentration maximum above the ODZ was likely the result of high rates of N_2O production from NO_2^- and NO_3^- reduction that are 10 – 100 fold higher than the rate of NH_4^+ oxidation to N_2O (Ji et al., 2015).

(3) Oxygen deficient zone (Figure S1c): $[O_2] < 5$ μmol L^{-1} and $[NO_2^-] > 1$ μmol L^{-1}, and depth = 70 – 400 m. The ODZ has prominent features such as the accumulation of NO_2^- (Codispoti and Christensen, 1985), and undersaturation of N_2O as a result of dynamic balance between the concomitant N_2O production (Ji et al., 2015) and consumption by denitrification (Babbin et al., 2015). The isotopic signature of "produced N_2O" had distinctively high $\delta^{15}N_{bulk}$ (8.5 ‰), and $\delta^{18}O$ (71 ‰, Table 1 and Figure S2), and this is indicative of pronounced N_2O reduction to N_2 which results in an isotope enrichment of the remaining N_2O pool in the process of N-O bond breakage (Toyoda et al., 2017). The SP signature was also high (39.9 ‰). While NH_4^+ oxidation can produce N_2O with similar SP values, we rule this out given the observed low O_2

concentrations (Peng et al., 2016). Instead, similar to the high $\delta^{15}N_{bulk}$ and $\delta^{18}O$ values which were observed, we suggest that the high SP values which were recorded in the ODZ, where N_2O undersaturation occurred, were also a result of N_2O consumption, as reduction of N_2O can also result in high SP values (Popp et al., 2002; Well et al., 2005; Mothet et al., 2013). Based on the observed $\delta^{15}N_{bulk}$, $\delta^{18}O$ and SP values of N_2O, we conclude that N_2O consumption was the predominant N_2O cycling pathway in the water body with $[O_2] < 5$ μmol L^{-1} and $[NO_2^-] > 1$ μmol L^{-1} in the ETSP.

(4) Intermediate waters (Figure S1d): Samples from depths 500 – 1000 m with $[O_2] = 5 – 70$ μmol L^{-1} and $[NO_2^-] < 1$ μmol L^{-1}. Generally, the N_2O concentration peak below the ODZ at the offshore waters can be found in this water body (Figure 4a). From the linear regression, the $SP_{produced}$ is 15.6±4.1 ‰, indicating both nitrification- and denitrification-produced N2O spanning the oxic and suboxic conditions ($[O_2] = 5 – 70$ μmol L^{-1}). Downward mixing and diffusion from ODZ is unlikely because the ETSP is a major upwelling region and ODZ samples had high SP values (see next paragraph). We conclude that localized N_2O production from nitrification and denitrification are important pathways in this region of the water column, and probably contributed to N_2O concentrations maxima in intermediate waters, as reported by Carrasco et al. (2017).

There are some limitations of the isotopomers-based analysis of potential N_2O production pathways. (1) Constant atmospheric exchange at the surface and mixed layer, and mesoscale eddy activities at intermediate waters (Arévalo-Martínez et al., 2016) could affect the $SP_{produced}$ from localized N_2O production. Nevertheless our conclusion of denitrification being important pathway remains valid. As a comparison, water bodies were divided by potential density surfaces (i.e. $\sigma_\theta > 27$ kg m^{-3}, 26 – 27 kg m^{-3}, 25 – 26 kg m^{-3}, < 25 kg m^{-3}) and showing $SP_{produced}$ of 5.0 – 11.1 ‰. (2) We are not able to investigate the change of N_2O production rates from nitrification and denitrification that are affected by El Niño-induced lower export production, as demonstrated by Espinoza-Morriberón et al. (2017). With complimentary dataset such as isotopic compositions of NO_3^- and NO_2^-, the rates of N_2O production can be derived by isotopic relationships during N_2O production processes using a three dimensional biogeochemical model (Bourbonnais et al., 2017).

4.2 The effect of O_2 on N_2O production from NH_4^+ oxidation

The surface and upper oxycline directly contribute to oceanic N_2O effluxes, with NH_4^+ oxidation being the dominant production pathway due to O_2 inhibition of denitrification (see section 4.1). Thus it is worth investigating N_2O production from NH_4^+ oxidation occurring along the oxygen gradient. During NH_4^+ oxidation to NO_2^-, the effectiveness of N_2O production can be quantified with the N_2O yield, which is defined as the molar nitrogen ratio of N_2O produced and NH_4^+ oxidized. In oxygenated waters, the near absence of NH_4^+ and NO_2^- suggest the amount of NH_4^+ oxidized produces equal amounts of NO_3^- within measurement error. Rees et al. (2011) and Grundle et al. (2012) computed the N_2O yield by deriving the slope of the linear regression of ΔN_2O-NO_3^- relationship. The ΔN_2O data from all sampling stations during October 2015 showed that ΔN_2O increases with increasing NO_3^- concentrations and decreasing O_2 concentrations (Figure 6). The samples from the upper oxycline ($[O_2] > 20$ μmol L^{-1} and depth < 500 m) showed moderate increase of ΔN_2O (0 – 20 nmol L^{-1}) when $[NO_3^-] < 20$ μmol L^{-1}. At $[NO_3^-] > 20$ μmol L^{-1}, substantial increase of ΔN_2O (20 – 75 nmol L^{-1}) was observed. Here, to

avoid sampling the ODZ where suboxic condition stimulates N_2O production from partial denitrification (i.e. water body (3) described in section 4.1), only data from the upper oxycline (depth < 500 m) were used to perform linear regression. The slope of the regression at $[NO_3^-] < 20$ µmol L^{-1} (corresponding to $[O_2] > 100$ µmol L^{-1}) is 0.85 ± 0.11, indicating that 0.085 ± 0.011 nmol of N_2O is produced for every µmol of NO_3^- produced (or NH_4^+ oxidized), equating to a molar nitrogen yield (mol N_2O-N produced / mol NO_3^- produced) of 0.17 ± 0.02 %. At $[NO_3^-] > 20$ µmol L^{-1} (corresponding to $[O_2] < 100$ µmol L^{-1}) the yield increases to 0.85 ± 0.13 %.

These N_2O yield estimates are generally comparable to previously reported values (0.04 – 1.6 %) in the ETSP (Elkins et al., 1978; Ji et al., 2015), and indicate that potential N_2O production from NH_4^+ oxidation decreases with water column oxygenation due to intrusion of oxygen-rich water masses (Llanillo et al., 2013; Graco et al., 2017), as well as El Niño-induced oxygenation (see section 4.3). As discussed earlier, the oxycline samples were probably influenced by mixing of suboxic water with active denitrification producing high N_2O concentrations and low NO_3^- concentrations; the N_2O yield estimates here are thus spatially and temporally integrated. As a comparison, ^{15}N tracer incubation method directly measured 0.04 % N_2O yield during NH_4^+ oxidation at $[O_2] > 100$ µmol L^{-1} (Ji et al., 2015).

4.3 N_2O distribution and fluxes during El Niño

Excess N_2O (ΔN_2O) in surface waters is one of the principal factors regulating N_2O fluxes. To evaluate the effect of strong El Niño events on oceanic N_2O fluxes, we compare surface and water column ΔN_2O concentrations in shelf waters (< 300 m depth) along 8 – 16 °S during El Niño (October 2015) and "neutral" conditions (December 2012). In the ETSP, Higher surface ΔN_2O concentrations and thus higher potential N_2O efflux occurred at near-shore waters. Generally, the surface ΔN_2O concentrations in October 2015 (Figure 7a) were lower than those of December 2012 (Figure 7d); highest surface ΔN_2O concentrations were 50 and 250 nmol L^{-1} in 2015 and 2012, respectively. The region of high surface ΔN_2O occurred at near ~ 14 °S and ~ 10 °S in 2015 and in 2012, respectively. It appears that N_2O efflux was significantly reduced during El Niño; in October 2015, coastal water had N_2O flux of 23 – 108 µmol m^{-2} d^{-1} (Figure 5c), much lower than that of December 2012 having 459 – 1825 µmol m^{-2} d^{-1} (Arévalo-Martínez et al., 2015). Such a 75 – 95 % reduction in N_2O fluxes during the 2015-16 El Niño was consistent with 80% reduction in fluxes observed during 1982-83 El Niño (Cline et al., 1987).

Suppressed upwelling or increased downwelling during El Niño events, as observed in both observational and model studies (Llanillo et al., 2013; Graco et al., 2017; Mogollón and Calil, 2017), can directly and indirectly affect N_2O fluxes to the atmosphere: First, reduced upward transport of subsurface N_2O-rich water not only decreased surface ΔN_2O, but also increased subsurface ΔN_2O, which is illustrated by the comparative observation of higher subsurface ΔN_2O concentrations in coastal waters in October 2015 (Figure 7b, 7c) than those in December 2012 (Figure 7e, 7f). Second, because the oxygen sensitivity of the denitrification sequence increases with each step (Körner and Zumft, 1989), El Niño-induced water column oxygenation inhibited N_2O consumption within the ODZ (bounded by $[O_2] = 5$ µmol L^{-1} isoline), as demonstrated by the disappearance of N_2O undersaturation ($\Delta N_2O < 0$) in coastal water in 2015 (Figure 7b, 7c), contrasting to water column N_2O

undersaturation occurring at 100 m at 13 – 14 °S in December 2012 (Figure 7e, 7f). Third, as shown in this study, the deepening and expansion of the suboxic zone caused by the El Niño event ($[O_2]$ = 5 – 20 µmol L^{-1}) stimulated subsurface N_2O production via denitrification, as demonstrated by the close spatial coupling between local maximum ΔN_2O concentrations and the oxycline ($[O_2]$ = 5 and 20 µmol L^{-1} isolines, Figure 7b and 7e). Lastly, upwelling of oxygen-rich water along the Peruvian coast, especially north of 12 °S (Stramma et al., 2016), inhibited local N_2O production and caused the southward relocation of surface ΔN_2O "hot spots".

The decrease of surface ΔN_2O concentration during El Niño was associated with an increase of subsurface N_2O concentrations. Water column ΔN_2O concentration profiles at expanded temporal and spatial coverage (see Figure 2a for location map, and Table S1 for coordinates) were compared within the same season between El Niño and non-El Niño years (Figure 8). We included N_2O data from January 2015 when the highest ONI was recorded during austral summer (Figure 1). These comparisons at offshore stations were made to cover the depth ranges with pronounced El Nino effects and available data (1000 m at station A and 800 m at station B and C). At coastal stations the depth ranges were station bottom depth (station D and E) or 250 m (station F). Generally, subsurface ΔN_2O concentration peaks were observed at deeper depths during 2015. Offshore stations had higher subsurface peak ΔN_2O concentrations during El Niño (Figure 8a, 8b), except at station C where the peak concentration during October 2015 was comparable to that of December 2012 (Figure 8c). At coastal stations D and E, higher ΔN_2O concentrations were found below 50 m but peak ΔN_2O concentrations were lower during El Niño years (Figure 8d, 8e). In the southernmost coastal station F, the peak ΔN_2O concentration was higher in 2015 than that of 1985; both were found at similar depths at ~ 60 m. The increase of subsurface N_2O concentrations during El Niño resulted in OMZ water column retaining larger amount of N_2O, as shown by higher depth-integrated N_2O concentrations during El Niño years than normal years in both coastal and offshore waters (Figure 9).

In all, the apparent decrease in N_2O efflux during strong El Niño events in the tropical Pacific, as shown in this study and others (Cline et al., 1987; Butler et al., 1989) is the result of complex physical and biochemical changes. The above comparative analyses are simple due to limited data availability. Consequently, these following aspects are yet to be resolved: (1) It is unclear how offshore N_2O fluxes vary from "neutral" to El Niño years. Current ΔN_2O profiles show higher surface ΔN_2O concentrations at station A and B in 2015 (Figure 8a and 8b), whereas the surface ΔN_2O was lower in 2015 at station C (Figure 8c). A zonal (east-west) section near 12 °S showed slightly higher offshore surface ΔN_2O in 2015 (~ 5 nmol L^{-1}, Figure 7c) than in 2012 (~ 1 nmol L^{-1}, Figure 7f). The decrease in coastal N_2O fluxes during El Niño could be compensated by increase in offshore fluxes. (2) The southward relocation of high surface ΔN_2O from neutral to El Niño years (Figure 7a and 7d) possibly results in higher surface ΔN_2O hence higher N_2O flux in southern region of ETSP (e.g. south of 16 °S, Figure 8f). (3) Complex hydrographical changes during the El Niño event resulted in the deepening of the ODZ boundary and the depths of peak N_2O concentration. It is possible that these chemical features occur in the similar potential density surfaces (with respect to non-El Niño conditions) that are deepened during El Niño, or they occur in different potential density surfaces during El Niño; or a combination of both. (4) It is possible that once the normal upwelling is resumed after the El Niño event, N_2O produced and retained in the subsurface layer in coastal and offshore

waters could be a potential reservoir contributing to high N_2O fluxes. (5) The co-occurrence of El Niño and mesoscale eddy formation along the Peruvian coast will have complicated effects on N_2O fluxes, which remains unexplored.

5 Conclusions

The eastern tropical South Pacific ocean is a major upwelling region with N_2O effluxes and active water column production affected by strong El Niño events. During a developing strong El Niño event in October 2015, a more pronounced warming effect occurred at lower latitudes in the ETSP. In comparison to conditions in December 2012 (non-El Niño), deepening of the oxygen deficient zone's upper boundary occurred at coastal waters in October 2015, coinciding with lower peak N_2O concentrations at deeper depths. Shelf N_2O effluxes were significantly lower during 2015 El Niño as a result of lower surface levels of N_2O supersaturation. However, a change of upwelling pattern appeared to cause higher subsurface N_2O concentrations and increased the water column N_2O inventories during El Niño than in other non-El Niño years. Natural abundance isotopic and isotopomer analysis indicated that both nitrification and denitrification are important pathways for N_2O production, and denitrification-derived N_2O probably contributes to the efflux to the atmosphere. Decreased N_2O efflux and subsurface accumulation during strong El Niño events is likely the result of suppressed upwelling and water column oxygenation. The current dataset represents a 'snapshot' of a developing El Niño event that lasted 18 months, thus the complex spatial and temporal patterns of El Niño-induced N_2O distribution in ETSP remain to be explored.

Figures and tables

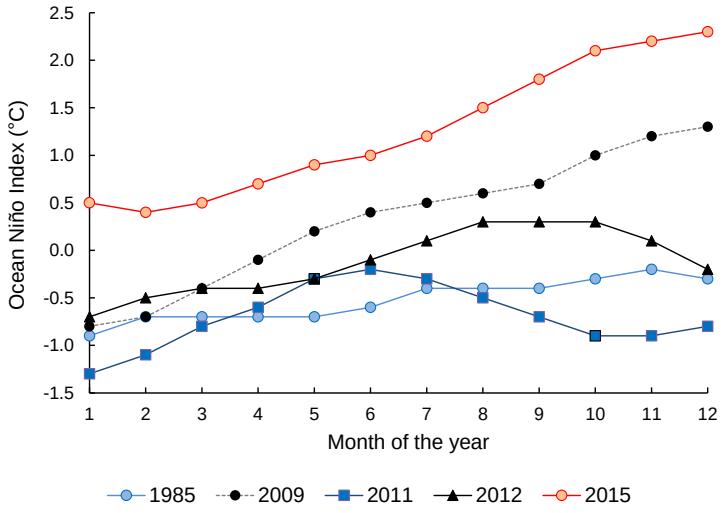

Figure 1: Ocean Niño Index of year 1985 (weak La Niña), 2009 (neutral), 2011 (weak La Niña), 2012 (neutral) and 2015 (strong El Niño). Data was downloaded from: http://origin.cpc.ncep.noaa.gov/products/analysis_monitoring/ensostuff/ONI_v5.php.

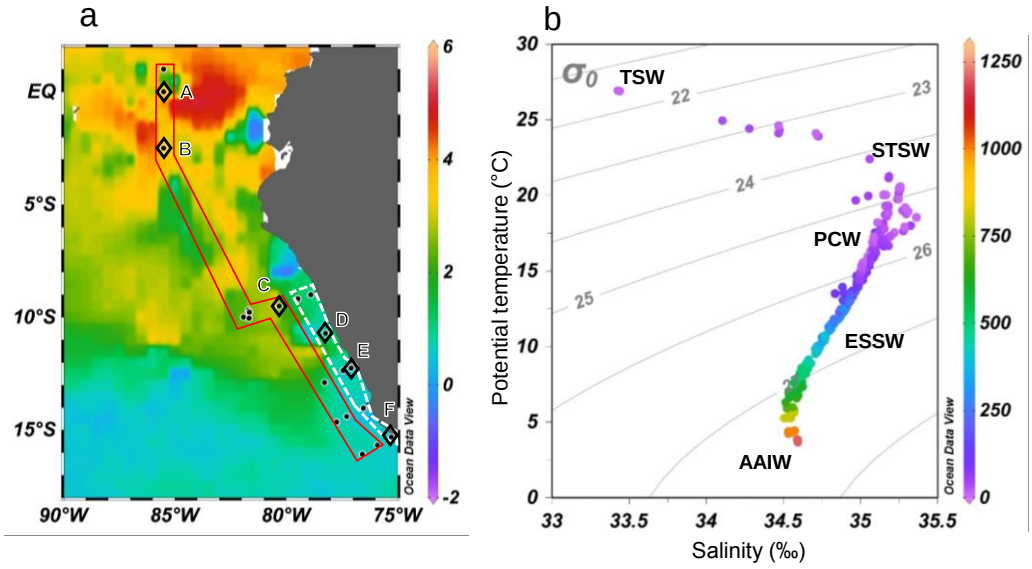

Figure 2: (a) Monthly mean sea surface temperature anomaly (℃) of October 2015 from NOAA's Satellite Coral Bleaching Monitoring Datasets. Sampling stations (filled circles) are categorized as "offshore" (in red polygon) and "coastal" sections (in white polygon). Comparative analyses of water column N_2O (see section 4.3) were performed at stations A – E (open diamonds). (b) Potential temperature – salinity diagram, with corresponding depths (meters, colour bar on right) and potential density (σ_0, kg m^{-3}) of all sampling stations. Five water masses are shown: Tropical surface water (TSW), Subtropical surface water (STSW), Peru coastal water (PCW), Equatorial subsurface water (ESSW) and Antarctic intermediate water (AAIW).

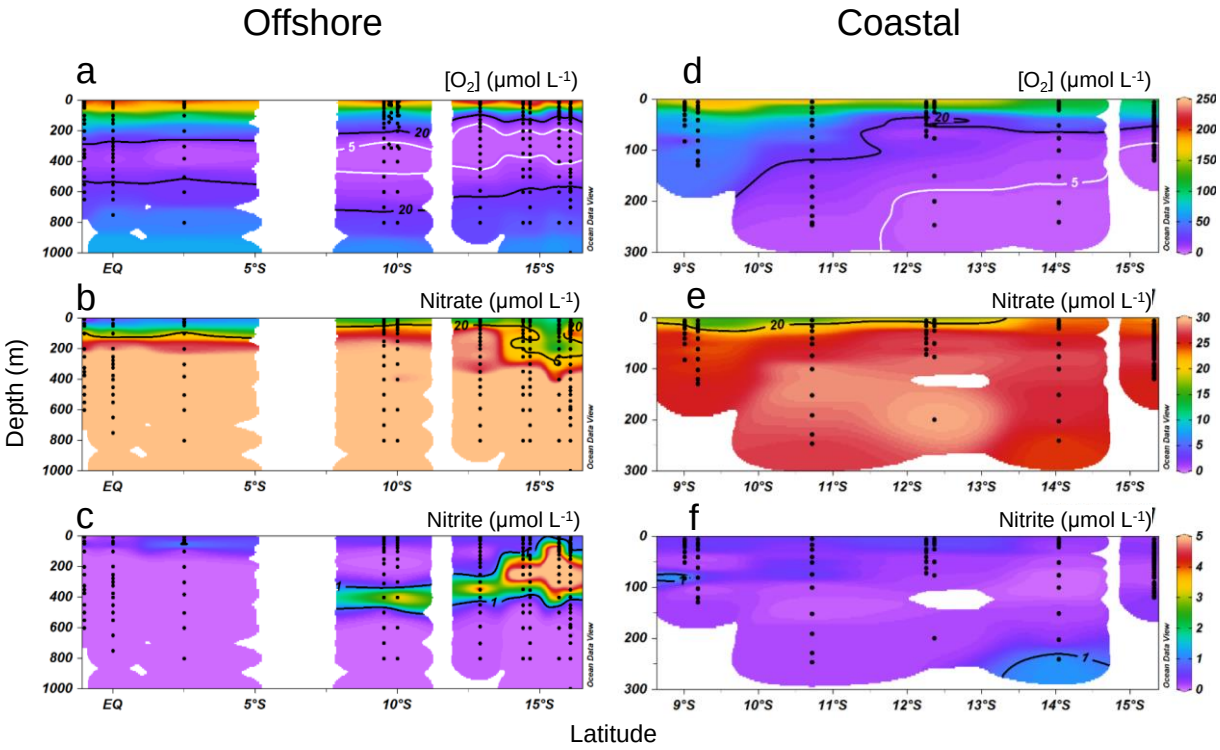

Figure 3: Water column oxygen (a and d), nitrate (b and e) and nitrite concentrations (c and f) along the offshore (a, b and c) and coastal sections (d, e and f) during October 2015.

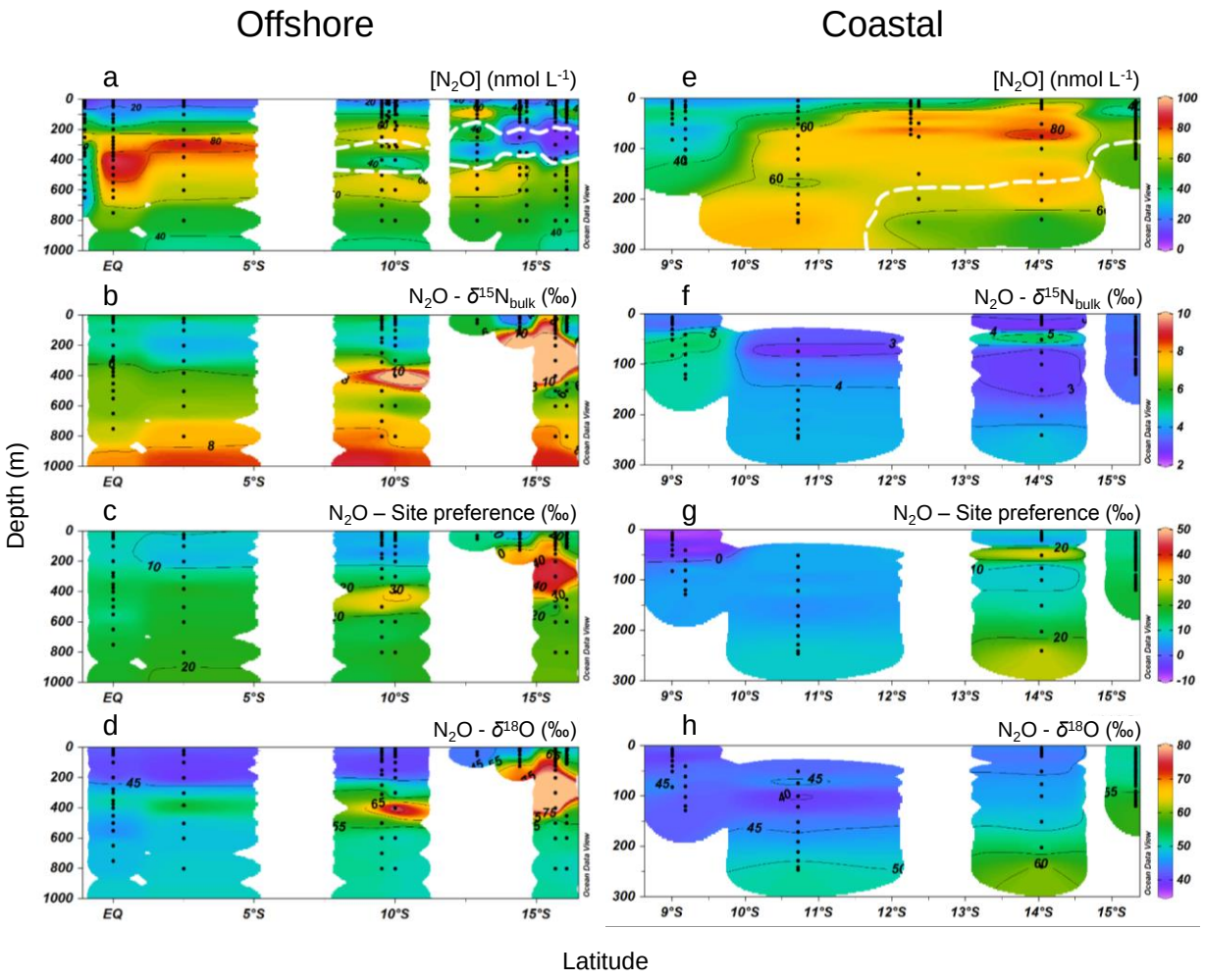

Figure 4: Water column N_2O concentrations (a and e), $\delta^{15}N_{bulk}$ (b and f), site preference (c and g) and $\delta^{18}O$ (d and h) along the offshore (a, b, c and d) and coastal sections (e, f, g and h) during October 2015. White contour line in (a) and (e) denote the boundary of oxygen deficient zone ($[O_2]$ = 5 µmol L^{-1} isoline).

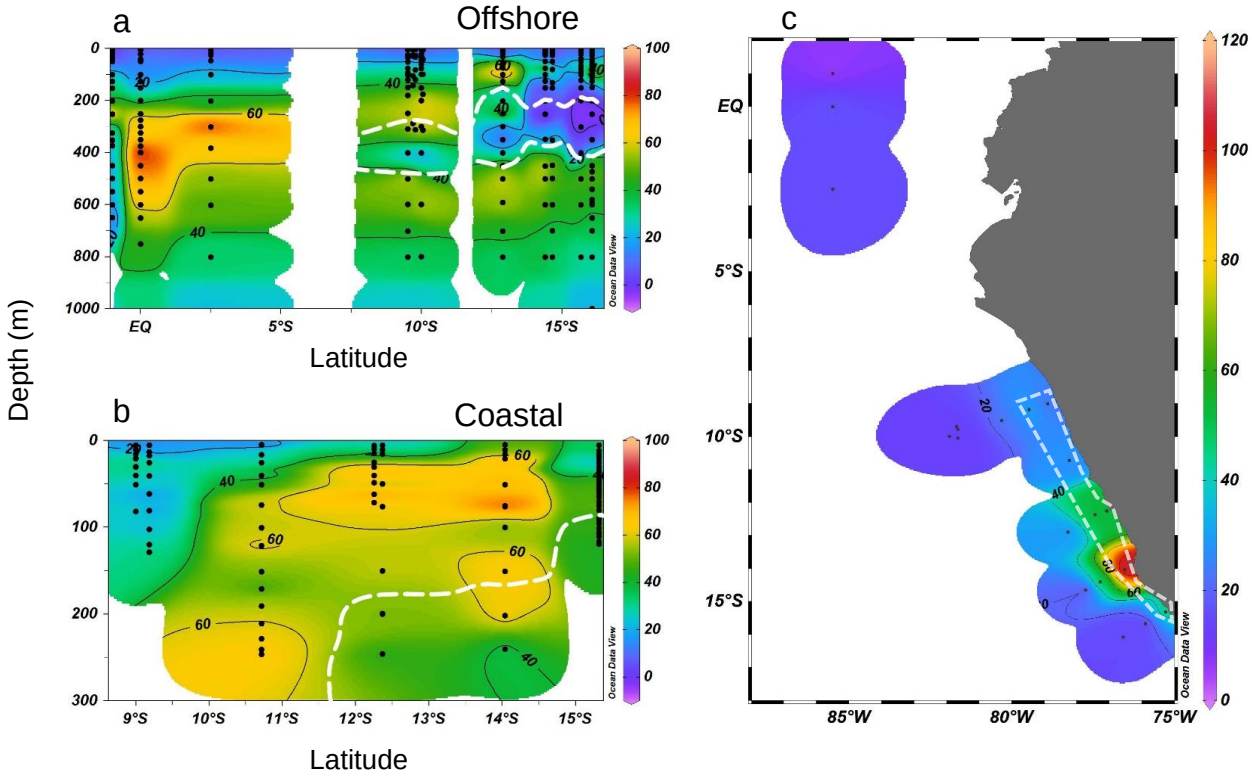

Figure 5: N_2O excess (ΔN_2O, nmol L^{-1}) at the offshore section (a) and the coastal section (b) during October 2015; the white dashed line indicates the boundary of the oxygen deficient zone ($[O_2]$ = 5 µmol L^{-1} isoline). (c) Surface N_2O efflux (µmol m^{-2} d^{-1}) from offshore and coastal stations (enclosed in white polygon) during October 2015.

5

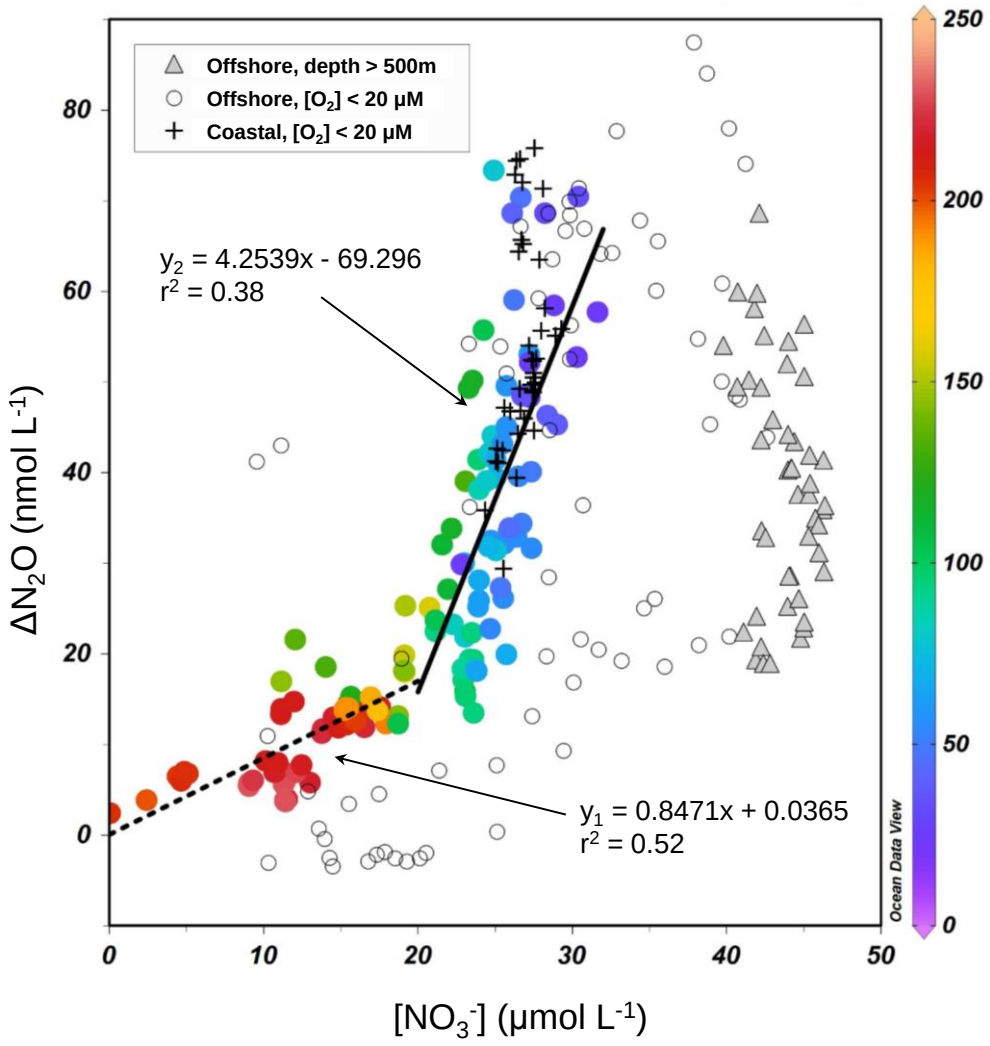

Figure 6: NO_3^--ΔN_2O relationship for samples from the upper oxycline ($[O_2]$ > 20 µmol L^{-1}, depth < 500 m, colored circles), low oxygen ($[O_2]$ < 20 µmol L^{-1}) coastal waters (+), low oxygen offshore waters (open circles), and the lower oxycline (depth > 500 m, filled triangles). Color bar shows the O_2 concentrations (µmol L^{-1}). For samples with NO_3^- concentrations higher and lower than 20 µmol L^{-1}, two linear regressions were performed separately.

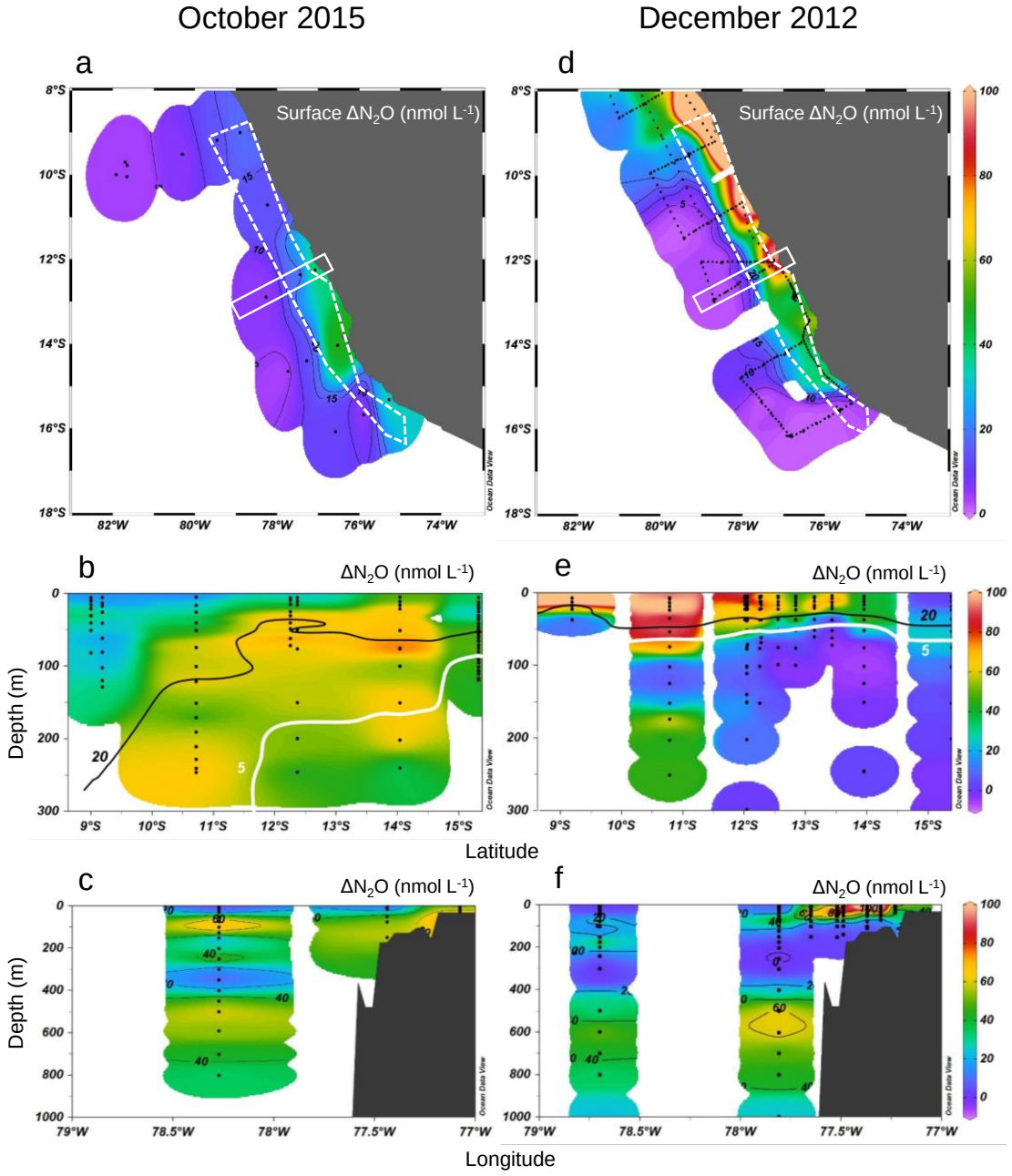

Figure 7: Surface ΔN_2O (a and d), meridional water column ΔN_2O distribution (b and e) and zonal water column ΔN_2O distribution (c and f) in October 2015 and in December 2012. Color bars for ΔN_2O (nmol L^{-1}) are shown in d, e and f. For meridional ΔN_2O distribution (b and e), data are from the coastal section, shown as white dashed polygon in panel (a) and (d). For zonal ΔN_2O distribution (c and f), data are from a section 12 – 13°S, shown as white rectangle. In (b) and (e) the "20" contour line (black) denotes the $[O_2]$ = 20 µmol L^{-1} isoline, equivalent to the lower boundary of oxygenated layer; the "5" contour line (white) denotes the $[O_2]$ = 5 µmol L^{-1} isoline, equivalent to the upper boundary of oxygen deficient zone.

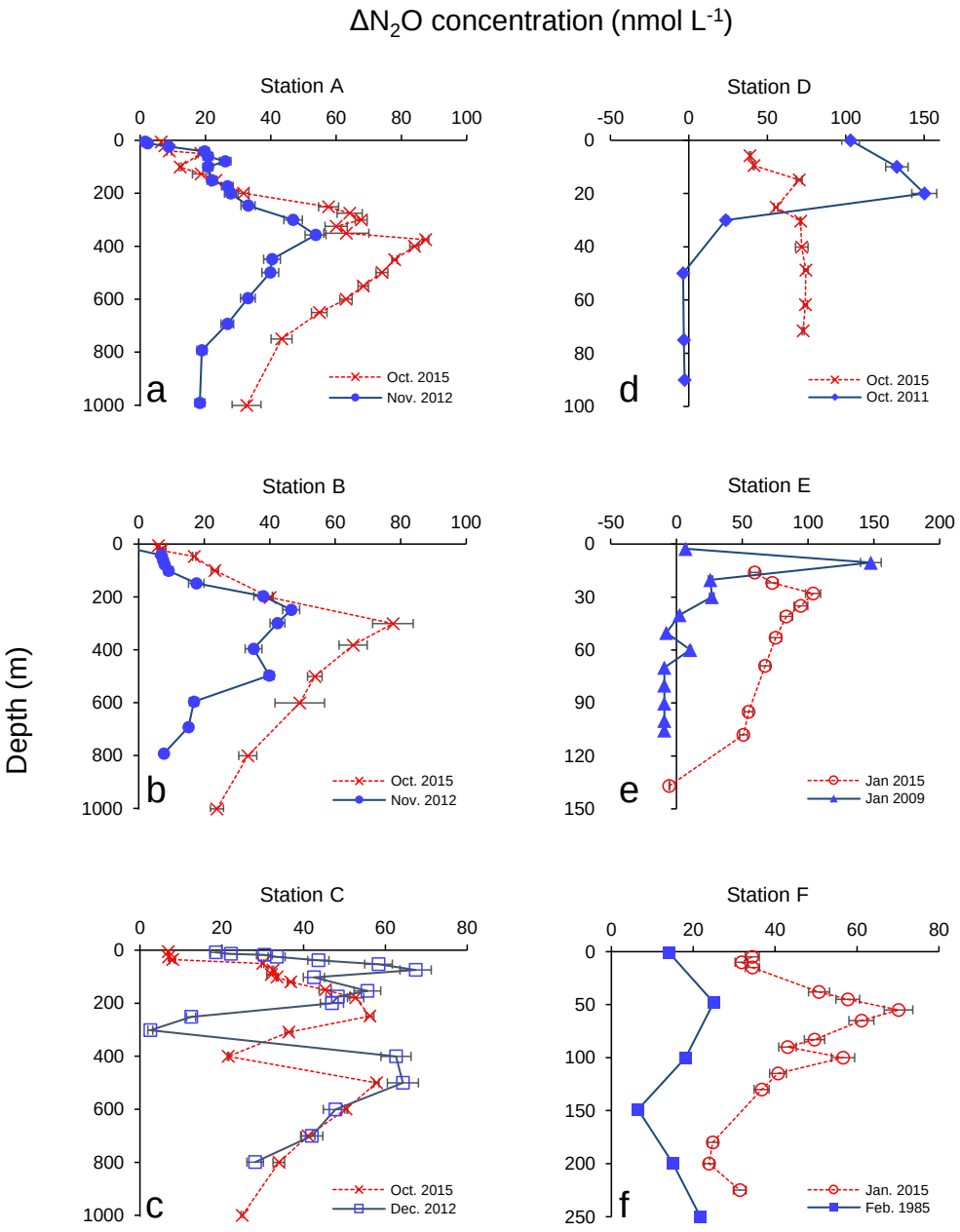

Figure 8: Depth profiles of N_2O concentration excess (ΔN_2O, nmol L^{-1}) measured at 6 different stations representing offshore (a, b and c) and coastal waters (d, e and f) during February 1985 (filled squares in f), January 2009 (filled triangles in e), October 2011 (filled diamonds in d), November 2012 (filled circles in a and b), December 2012 (open squares in c), January 2015 (open circles in e and f) and October 2015 (crosses). Profiles of 2015 are indicated in red and other years in blue. Error bars of October 2015 data represent standard deviation of triplicate measurements; error bars of the other profiles (from MEMENTO database) represent 5% of the N_2O concentration measurements.

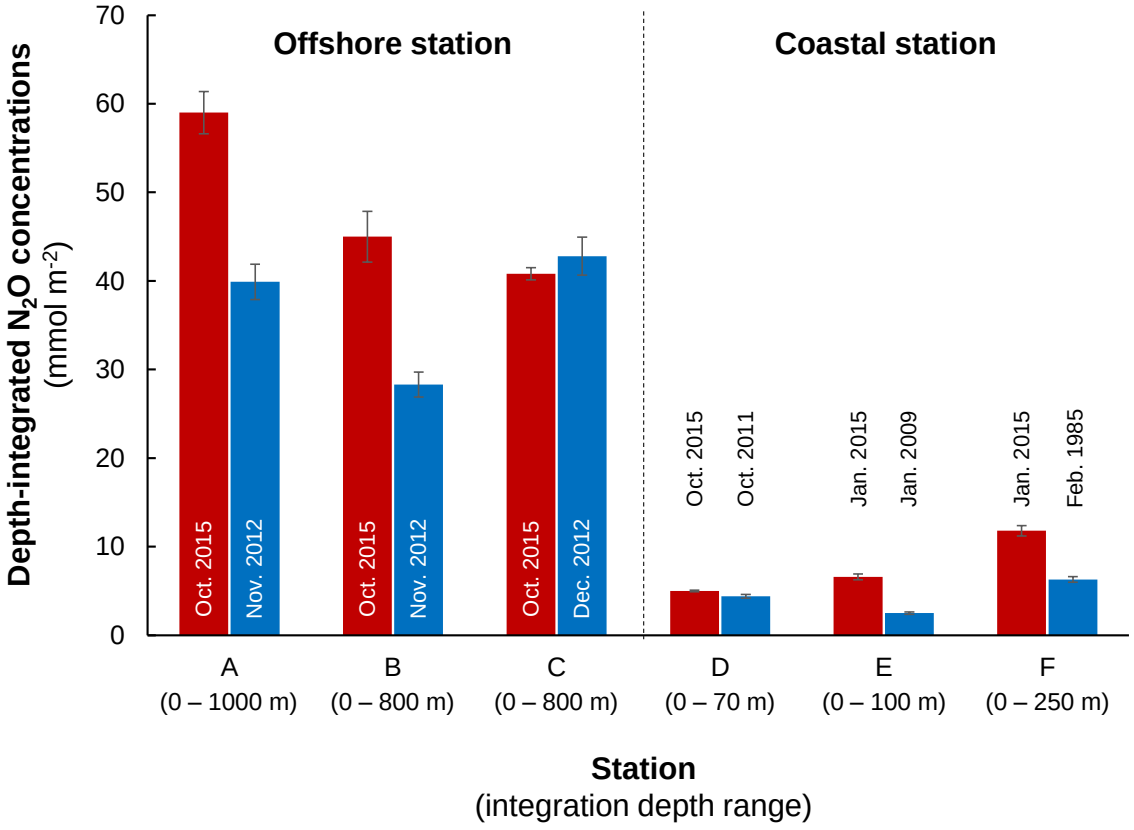

Figure 9 Comparison of depth-integrated N_2O concentrations between El Niño (red bars) and normal years (blue bars). Station A, B and C are characterized as offshore stations whereas D, E and F are as coastal stations. See Figure 2a for station locations and Table S1 for references.

5

Table 1: Isotopic signature of produced N_2O estimated by linear regression of isotopomer ratios and inverse N_2O concentrations (see section 4.1 for model description and supplementary Figure S1 for results) in ODZ, N_2O peak, oxycline and surface layers.

No.	Layer	Definition	Statistical properties	$\delta^{15}N_{bulk}$ (‰)	$\delta^{18}O$ (‰)	SP (‰)
1	Upper oxycline and surface	Depth 0 – 200 m $[O_2] > 5$ µmol L^{-1} $[NO_2^-] < 1$ µmol L^{-1}	Produced N_2O	2.8	45.9	6.4
			Standard error	0.3	1.2	1.9
			R^2 (n = 76)	0.37	0	0.04
2	N_2O peak	Depth = 45 – 500 m $[O_2] = 5 – 20$ µmol L^{-1} $[NO_2^-] < 1$ µmol L^{-1}	Produced N_2O	5.4	41.3	8.3
			Standard error	0.9	3.0	3.0
			R^2 (n = 48)	0.04	0.24	0.08
3	Oxygen deficient zone	Depth = 70 – 400 m $[O_2] < 5$ µmol L^{-1} $[NO_2^-] > 1$ µmol L^{-1}	Produced N_2O	8.5	71.0	39.9
			Standard error	1.5	4.5	4.4
			R^2 (n = 11)	0.38	0.40	0.01
4	Intermediate waters	Depth = 500 – 1000 m $[O_2] = 5 – 70$ µmol L^{-1} $[NO_2^-] < 0.02$ µmol L^{-1}	Produced N_2O	3.6	50.0	15.6
			Standard error	0.6	2.4	4.1
			R^2 (n = 21)	0.69	0	0.04

Acknowledgements

The German Federal Ministry of Education and Research (BMBF) grant (03G0243A) awarded to C. Marandino, D. Grundle and T. Steinhoff supported the ASTRA-OMZ cruise onboard the R/V Sonne in October 2015. The German Science Foundation (DFG) provided support via the Collaborative Research Centre 754: Climate-Biogeochemistry Interactions in the Tropical Ocean and funded the R/V Meteor cruises. The BMBF also supported this study as part of the SOPRAN project I and II (03F0611A, 03F0662A). We thank the captains and crews of the R/V Meteor and R/V Sonne cruises for their help, C. Marandino (co-chief scientist) and T. Steinhoff for co-organizing the R/V Sonne cruise with D. Grundle, and M. Lohmann, H. Campen and M. Sun for the oxygen and nutrient measurements and help with N_2O sampling. We thank the Peruvian authorities for allowing us to conduct work in their territorial waters. We thank Tina Baustian contributing hydrography and N_2O data off the Peruvian coast. In preparation of the manuscript, C. Marandino and L. Stramma provided constructive comments. Ji also received support from DFG (GR4731/2-1 and MA6297/3-1) awarded to D. Grundle and C. Marandino.

Data availability

Raw data presented in this manuscript can be found in the Supplementary material.

Author contributions

DSG developed the experimental design and was co-PI and co-Chief Scientist of the ASTRA-OMZ cruise. HWB, MIG, XM, DLA-M, and DSG conducted field sampling. DG, MA, XM, DLA-M conducted laboratory analyses. QJ and DSG performed data synthesis. QJ, MA, HWB, MIG, XM, DLA-M, DSG prepared the manuscript.

Competing Interests

The authors declare that they have no conflict of interest.

References

Anderson, J. H.: The metabolism of hydroxylamine to nitrite by Nitrosomonas, The Biochemical Journal, 91, 8-17, 1964.

Arévalo-Martínez, D. L., Kock, A., Loscher, C. R., Schmitz, R. A., and Bange, H. W.: Massive nitrous oxide emissions from the tropical South Pacific Ocean, Nat. Geosci., 8, 530-533, doi:10.1038/ngeo2469, 2015.

Arévalo-Martínez, D. L., Kock, A., Löscher, C. R., Schmitz, R. A., Stramma, L., and Bange, H. W.: Influence of mesoscale eddies on the distribution of nitrous oxide in the eastern tropical South Pacific, Biogeosciences, 13, 1105-1118, doi:10.5194/bg-13-1105-2016, 2016.

Babbin, A. R., Bianchi, D., Jayakumar, A., and Ward, B. B.: Rapid nitrous oxide cycling in the suboxic ocean, Science, 348, 1127-1129, doi:10.1126/science.aaa8380, 2015.

Barber, R. T., and Chavez, F. P.: Biological Consequences of El Niño, Science, 222, 1203-1210, doi:10.1126/science.222.4629.1203, 1983.

Blasing, T.: Recent greenhouse gas concentrations, Carbon Dioxide Information Analysis Center (CDIAC), Oak Ridge National Laboratory (ORNL), Oak Ridge, TN (United States), 2016.

Bonin, P., Gilewicz, M., and Bertrand, J. C.: Effects of oxygen on each step of denitrification on Pseudomonas nautica, Can. J. Microbiol., 35, 1061-1064, doi:10.1139/m89-177, 1989.

Bourbonnais, A., Letscher, R. T., Bange, H. W., Échevin, V., Larkum, J., Mohn, J., Yoshida, N., and Altabet, M. A.: N2O production and consumption from stable isotopic and concentration data in the Peruvian coastal upwelling system, Glob. Biogeochem. Cycles., 31, 678-698, doi:10.1002/2016GB005567, 2017.

Butler, J. H., Elkins, J. W., Thompson, T. M., and Egan, K. B.: Tropospheric and dissolved N2O of the west Pacific and east Indian Oceans during the El Niño Southern Oscillation event of 1987, J Geophys. Res. Atmos., 94, 14865-14877, doi:10.1029/JD094iD12p14865, 1989.

Carrasco, C., Karstensen, J., and Farias, L.: On the Nitrous Oxide Accumulation in Intermediate Waters of the Eastern South Pacific Ocean, Front. Mar. Sci., 4, doi:10.3389/fmars.2017.00024, 2017.

Chavez, F. P., Ryan, J., Lluch-Cota, S. E., and Ñiquen C., M.: From Anchovies to Sardines and Back: Multidecadal Change in the Pacific Ocean, Science, 299, 217-221, doi:10.1126/science.1075880, 2003.

Cline, J. D., Wisegarver, D. P., and Kelly-Hansen, K.: Nitrous oxide and vertical mixing in the equatorial Pacific during the 1982–1983 El Niño, Deep. Sea. Res., 34, 857-873, doi:http://dx.doi.org/10.1016/0198-0149(87)90041-0, 1987.

Codispoti, L. A., and Christensen, J. P.: Nitrification, denitrification and nitrous oxide cycling in the eastern tropical South Pacific ocean, Mar. Chem., 16, 277-300, doi:10.1016/0304-4203(85)90051-9, 1985.

Cornejo, M., Murillo, A. A., and Farías, L.: An unaccounted for N2O sink in the surface water of the eastern subtropical South Pacific: Physical versus biological mechanisms, Prog. Oceanogr., 137, 12-23, doi:https://doi.org/10.1016/j.pocean.2014.12.016, 2015.

Elkins, J. W., Steven C. Wofsy, Michael B. Mcelroy, Charles E. Kolb, and Kaplan, W. A.: Aquatic sources and sinks for nitrous oxide, Nature, 275, 602-606, doi:10.1038/275602a0, 1978.

Espinoza-Morriberón, D., Echevin, V., Colas, F., Tam, J., Ledesma, J., Vásquez, L., and Graco, M.: Impacts of El Niño events on the Peruvian upwelling system productivity, J. Geophys. Res. Oceans, 122, 5423-5444, doi:10.1002/2016JC012439, 2017.

Farías, L., Castro-González, M., Cornejo, M., Charpentier, J., Faúndez, J., Boontanon, N., and Yoshida, N.: Denitrification and nitrous oxide cycling within the upper oxycline of the eastern tropical South Pacific oxygen minimum zone, Limnol. Oceanogr., 54, 132-144, doi:10.4319/lo.2009.54.1.0132, 2009.

Farías, L., Faúndez, J., Fernández, C., Cornejo, M., Sanhueza, S., and Carrasco, C.: Biological N2O Fixation in the Eastern South Pacific Ocean and Marine Cyanobacterial Cultures, PLOS ONE, 8, e63956, doi:10.1371/journal.pone.0063956, 2013.

Frame, C. H., and Casciotti, K. L.: Biogeochemical controls and isotopic signatures of nitrous oxide production by a marine ammonia-oxidizing bacterium, Biogeosciences, 7, 2695-2709, doi:https://doi.org/10.5194/bg-7-2695-2010, 2010.

Fujii, A., Toyoda, S., Yoshida, O., Watanabe, S., Sasaki, K. i., and Yoshida, N.: Distribution of nitrous oxide dissolved in water masses in the eastern subtropical North Pacific and its origin inferred from isotopomer analysis, Journal of Oceanography, 69, 147-157, doi:10.1007/s10872-012-0162-4, 2013.

Garcia, H. E., and Gordon, L. I.: Oxygen solubility in seawater: Better fitting equations, Limnol. Oceanogr., 6, 1307-1312, 1992.

Graco, M. I., Purca, S., Dewitte, B., Castro, C. G., Morón, O., Ledesma, J., Flores, G., and Gutiérrez, D.: The OMZ and nutrient features as a signature of interannual and low-frequency variability in the Peruvian upwelling system, Biogeosciences, 14, 4601-4617, doi:10.5194/bg-14-4601-2017, 2017.

Grundle, D. S., Maranger, R., and Juniper, S. K.: Upper Water Column Nitrous Oxide Distributions in the Northeast Subarctic Pacific Ocean, Atmosphere-Ocean, 50, 475-486, doi:10.1080/07055900.2012.727779, 2012.

Grundle, D. S., Löscher, C. R., Krahmann, G., Altabet, M. A., Bange, H. W., Karstensen, J., Körtzinger, A., and Fiedler, B.: Low oxygen eddies in the eastern tropical North Atlantic: Implications for N2O cycling, Scientific Reports, 7, 4806, doi:10.1038/s41598-017-04745-y, 2017.

Haskell, W. Z., Kadko, D., Hammond, D. E., Knapp, A. N., Prokopenko, M. G., Berelson, W. M., and Capone, D. G.: Upwelling velocity and eddy diffusivity from 7Be measurements used to compare vertical nutrient flux to export POC flux in the Eastern Tropical South Pacific, Mar. Chem., 168, 140-150, doi:https://doi.org/10.1016/j.marchem.2014.10.004, 2015.

Ji, Q., Babbin, A. R., Jayakumar, A., Oleynik, S., and Ward, B. B.: Nitrous oxide production by nitrification and denitrification in the Eastern Tropical South Pacific oxygen minimum zone, Geophys. Res. Lett., 42, 10,755-710,764, doi:10.1002/2015GL066853, 2015.

Kock, A., and Bange, H. W.: Counting the ocean's greenhouse gas emissions, Eos, 10-13, doi:10.1029/2015EO023665, 2015.

Kock, A., Arevalo-Martinez, D. L., Löscher, C., and Bange, H. W.: Extreme N2O accumulation in the coastal oxygen minimum zone off Peru, Biogeosciences (BG), 13, 827-840, 2016.

Körner, H., and Zumft, W. G.: Expression of denitrification enzymes in response to the dissolved oxygen level and respiratory substrate in continuous culture of Pseudomonas stutzeri, Appl. Environ. Microbiol., 55, 1670-1676, 1989.

Llanillo, P. J., Karstensen, J., Pelegrí, J. L., and Stramma, L.: Physical and biogeochemical forcing of oxygen and nitrate changes during El Niño/El Viejo and La Niña/La Vieja upper-ocean phases in the tropical eastern South Pacific along 86°W, Biogeosciences, 10, 6339-6355, doi:10.5194/bg-10-6339-2013, 2013.

Mogollón, R., and Calil, P. H. R.: On the effects of ENSO on ocean biogeochemistry in the Northern Humboldt Current System (NHCS): A modeling study, Journal of Marine Systems, 172, 137-159, doi:https://doi.org/10.1016/j.jmarsys.2017.03.011, 2017.

Mohn, J., Wolf, B., Toyoda, S., Lin, C.-T., Liang, M.-C., Brüggemann, N., Wissel, H., Steiker Amy, E., Dyckmans, J., Szwec, L., Ostrom Nathaniel, E., Casciotti Karen, L., Forbes, M., Giesemann, A., Well, R., Doucett Richard, R., Yarnes Chris, T., Ridley Anna, R., Kaiser, J., and Yoshida, N.: Interlaboratory assessment of nitrous oxide isotopomer analysis by isotope ratio mass spectrometry and laser spectroscopy: current status and perspectives, Rapid Communications in Mass Spectrometry, 28, 1995-2007, doi:10.1002/rcm.6982, 2014.

Mothet, A., Sebilo, M., Laverman, A. M., Vaury, V., and Mariotti, A.: Is site preference of N2O a tool to identify benthic denitrifier N2O?, Environmental Chemistry, 10, 281-284, 2013.

Ñiquen, M., and Bouchon, M.: Impact of El Niño events on pelagic fisheries in Peruvian waters, Deep Sea Res Part 2 Top Stud Oceanogr, 51, 563-574, doi:https://doi.org/10.1016/j.dsr2.2004.03.001, 2004.

Peng, X., Fuchsman, C. A., Jayakumar, A., Warner, M. J., Devol, A. H., and Ward, B. B.: Revisiting nitrification in the Eastern Tropical South Pacific: A focus on controls, J. Geophys. Res. Oceans, 121, 1667-1684, doi:10.1002/2015JC011455, 2016.

Philander, S. G. H.: El Nino Southern Oscillation phenomena, Nature, 302, 295-301, 1983.

Popp, B. N., Westley, M. B., Toyoda, S., Miwa, T., Dore, J. E., Yoshida, N., Rust, T. M., Sansone, F. J., Russ, M. E., Ostrom, N. E., and Ostrom, P. H.: Nitrogen and oxygen isotopomeric constraints on the origins and sea-to-air flux of N2O in the oligotrophic subtropical North Pacific gyre, Glob. Biogeochem. Cycles., 16, 12-11-12-10, doi:doi:10.1029/2001GB001806, 2002.

Ravishankara, A., Daniel, J. S., and Portmann, R. W.: Nitrous oxide (N2O): the dominant ozone-depleting substance emitted in the 21st century, Science, 326, 123-125, 2009.

Rees, A. P., Brown, I. J., Clark, D. R., and Torres, R.: The Lagrangian progression of nitrous oxide within filaments formed in the Mauritanian upwelling, Geophys. Res. Lett., 38, L21606, doi:doi:10.1029/2011GL049322, 2011.

Revsbech, N. P., Larsen, L. H., Gundersen, J., Dalsgaard, T., Ulloa, O., and Thamdrup, B.: Determination of ultra-low oxygen concentrations in oxygen minimum zones by the STOX sensor, Limnol Oceanogr. Meth., 7, 371-381, 2009.

Santoso, A., Mcphaden, M. J., and Cai, W.: The defining characteristics of ENSO extremes and the strong 2015/2016 El Niño, Reviews of Geophysics, 55, 1079-1129, 2017.

Silva, N., Rojas, N., and Fedele, A.: Water masses in the Humboldt Current System: Properties, distribution, and the nitrate deficit as a chemical water mass tracer for Equatorial Subsurface Water off Chile, Deep Sea Res Part 2 Top Stud Oceanogr, 56, 1004-1020, 2009.

Stramma, L., Fischer, T., Grundle, D. S., Krahmann, G., Bange, H. W., and Marandino, C. A.: Observed El Niño conditions in the eastern tropical Pacific in October 2015, Ocean Sci., 12, 861-873, doi:10.5194/os-12-861-2016, 2016.

Strub, P. T., Mesías, J. M., Montecino, V., Rutillant, J., and Salinas, S.: Coastal ocean circulation off western south America,, in: The Sea, edited by: Robinson, A. R., and Brink, K. H., John Wiley, New York, 273-313, 1998.

Toyoda, S., Yano, M., Nishimura, S.-i., Akiyama, H., Hayakawa, A., Koba, K., Sudo, S., Yagi, K., Makabe, A., Tobari, Y., Ogawa, N. O., Ohkouchi, N., Yamada, K., and Yoshida, N.: Characterization and production and consumption processes of N2O emitted from temperate agricultural soils determined via isotopomer ratio analysis, Glob. Biogeochem. Cycles., 25, n/a-n/a, doi:10.1029/2009GB003769, 2011.

Toyoda, S., Yoshida, N., and Koba, K.: Isotopocule analysis of biologically produced nitrous oxide in various environments, Mass Spectrom. Rev., 36, 135-160, 2017.

Trimmer, M., Chronopoulou, P.-M., Maanoja, S. T., Upstill-Goddard, R. C., Kitidis, V., and Purdy, K. J.: Nitrous oxide as a function of oxygen and archaeal gene abundance in the North Pacific, Nat. Commun., 7, 13451, doi:https://doi.org/10.1038/ncomms13451, 2016.

Walter, S., Breitenbach, U., Bange, H. W., Nausch, G., and Wallace, D. W. R.: Distribution of N2O in the Baltic Sea during transition from anoxic to oxic conditions, Biogeosciences, 3, 557-570, doi:10.5194/bg-3-557-2006, 2006.

Wanninkhof, R.: Relationship between wind speed and gas exchange over the ocean revisited, Limnology and Oceanography: Methods, 12, 351-362, doi:doi:10.4319/lom.2014.12.351, 2014.

Weiss, R. F., and Price, B. A.: Nitrous oxide solubility in water and seawater, Mar. Chem., 8, 347-359, doi:https://doi.org/10.1016/0304-4203(80)90024-9, 1980.

Well, R., Flessa, H., Jaradat, F., Toyoda, S., and Yoshida, N.: Measurement of isotopomer signatures of N2O in groundwater, J Geophys. Res. Biogeosci., 110, doi:doi:10.1029/2005JG000044, 2005.

Winther, M., Balslev-Harder, D., Christensen, S., Priemé, A., Elberling, B., Crosson, E., and Blunier, T.: Continuous measurements of nitrous oxide isotopomers during incubation experiments, Biogeosciences, 15, 767-780, doi:10.5194/bg-15-767-2018, 2018.

Yamagishi, H., Westley, M. B., Popp, B. N., Toyoda, S., Yoshida, N., Watanabe, S., Koba, K., and Yamanaka, Y.: Role of nitrification and denitrification on the nitrous oxide cycle in the eastern tropical North Pacific and Gulf of California, J Geophys. Res. Biogeosci., 112, n/a-n/a, doi:10.1029/2006JG000227, 2007.

Yang, S., Gruber, N., Long, M. C., and Vogt, M.: ENSO-Driven Variability of Denitrification and Suboxia in the Eastern Tropical Pacific Ocean, Glob. Biogeochem. Cycles., 31, 1470-1487, doi:doi:10.1002/2016GB005596, 2017.

Yoshida, N., and Toyoda, S.: Constraining the atmospheric N2O budget from intramolecular site preference in N2O isotopomers, Nature, 405, 330, doi:10.1038/35012558, 2000.